Mesoscale spatial variability of lower thermospheric winds during the Anomalous Transport Experiment (ATREX)

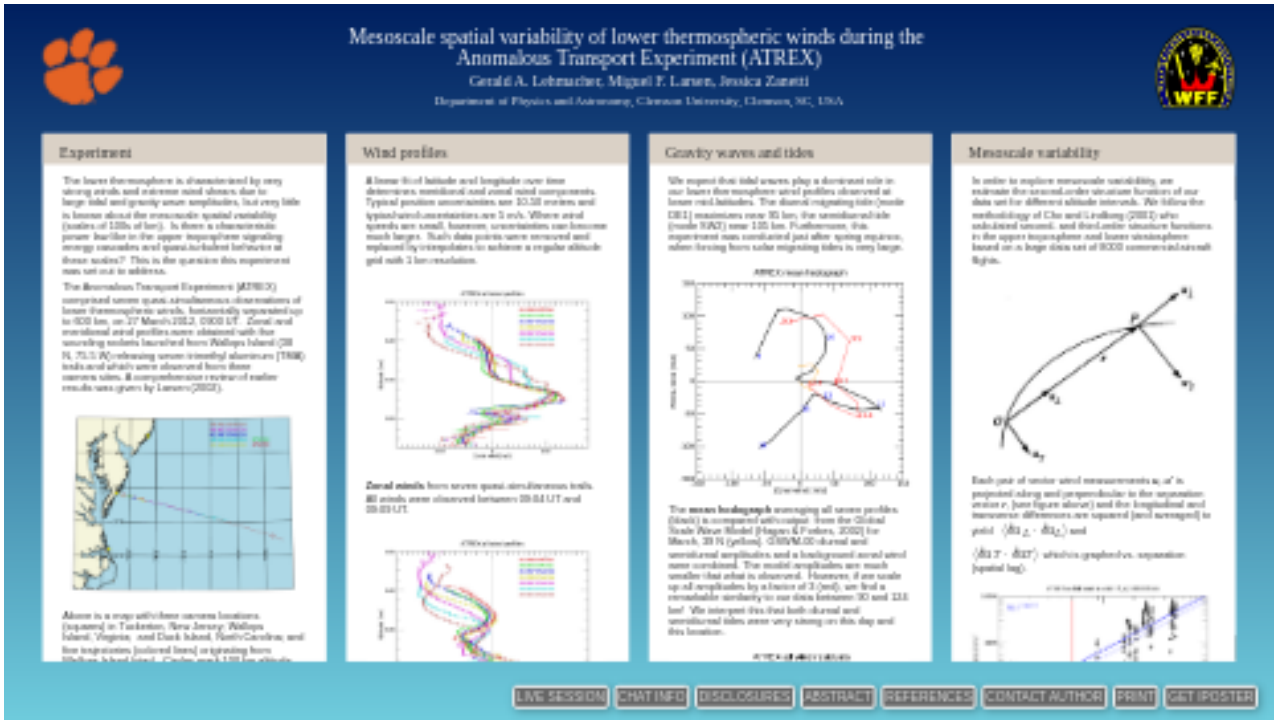

Gerald A. Lehmacher, Miguel F. Larsen, Jessica Zanetti

Department of Physics and Astronomy, Clemson University, Clemson, SC, USA

PRESENTED AT:

AGU FALL MEETING
Online Everywhere | 1–17 December 2020

EXPERIMENT

The lower thermosphere is characterized by very strong winds and extreme wind shears due to large tidal and gravity wave amplitudes, but very little is known about the mesoscale spatial variability (scales of 100s of km). Is there a characteristic power law like in the upper troposphere signaling energy cascades and quasi-turbulent behavior at these scales? This is the question this experiment was set out to address.

The Anomalous Transport Experiment (ATREX) comprised seven quasi-simultaneous observations of lower thermospheric winds, horizontally separated up to 600 km, on 27 March 2012, 0900 UT. Zonal and meridional wind profiles were obtained with five sounding rockets launched from Wallops Island (38 N, 75.5 W) releasing seven trimethyl aluminum (TMA) trails and which were observed from three camera sites. A comprehensive review of earlier results was given by Larsen (2002).

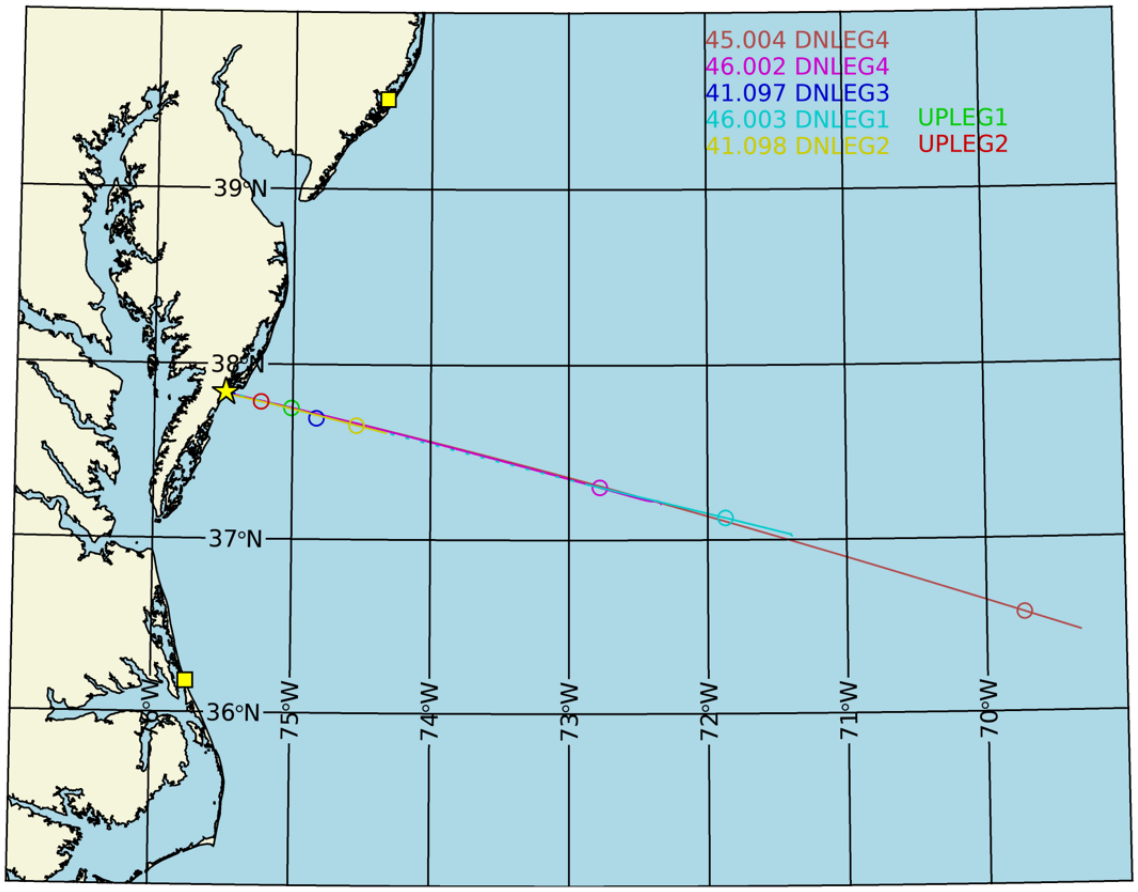

Above is a map with three camera locations (squares) in Tuckerton, New Jersey; Wallops Island, Virginia; and Duck Island, North Carolina; and five trajectories (colored lines) originating from Wallops Island (star). Circles mark 100 km altitude crossings.

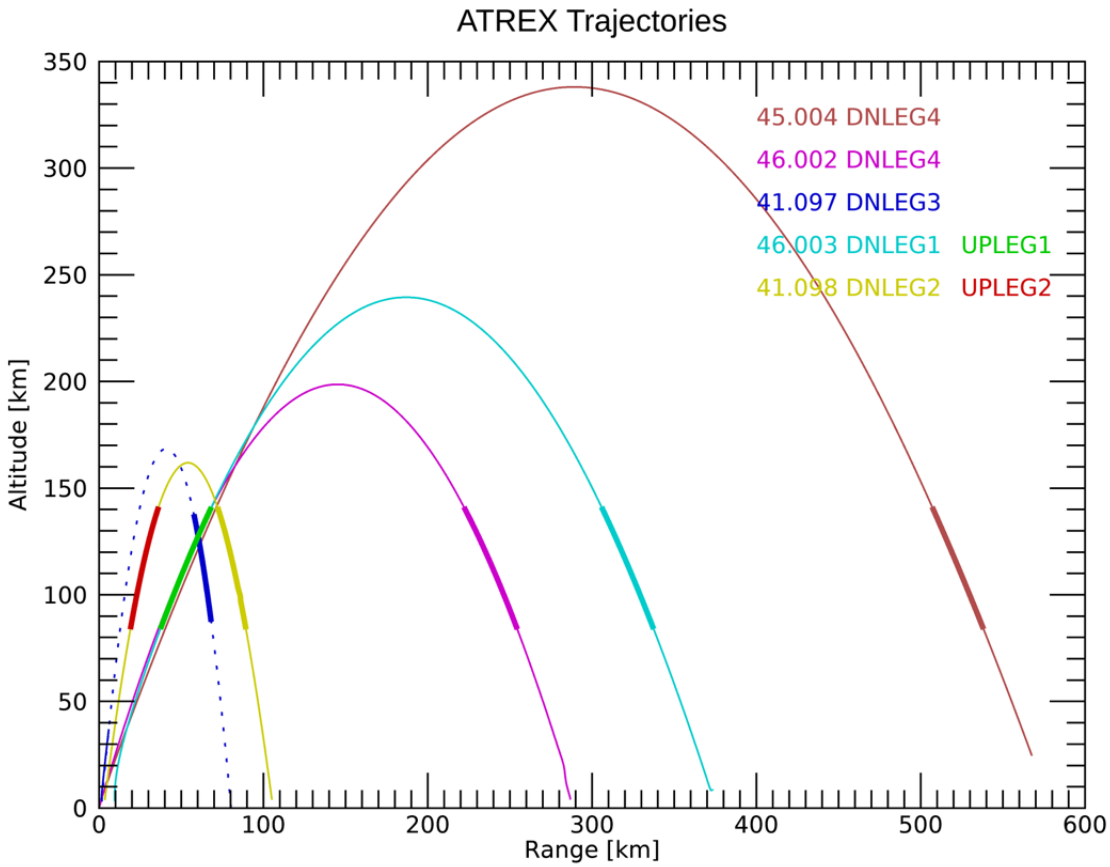

The observed trajectories for five suborbital payloads, denominated by their 5-digit NASA mission number. (Due to radar constraints, 41.097 (dark blue) was only tracked during the early ascent.) Thicker lines mark the nominal heights of TMA release (90-140 km). Launch times were staggered within a 10-minute interval, so that trail releases occurred quasi-simultaneously.

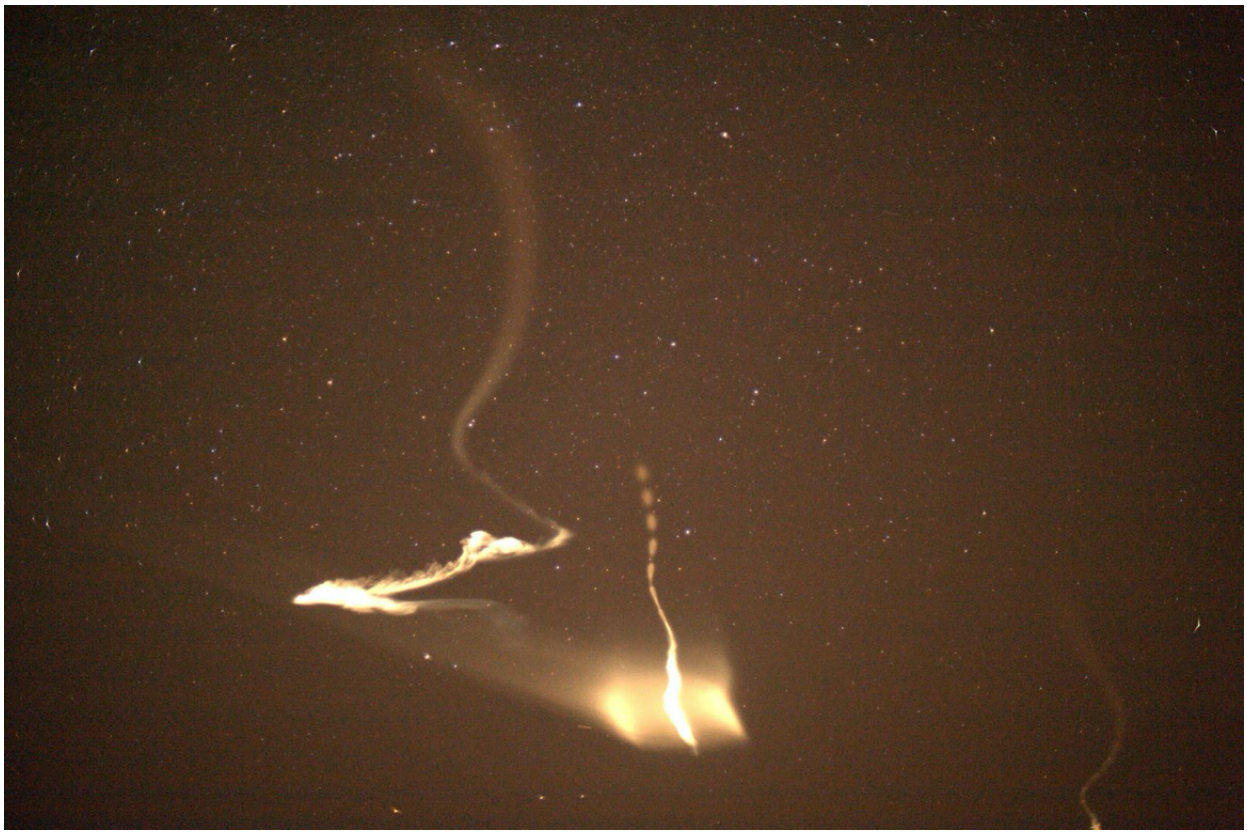

Images weren taken every five seconds synchronized between the camera sites, which were equipped with three digital cameras each covering different field-of-views to capture all trails. Here is an example image seen from Duck Island. In the foreground to the left is an upleg trail that has already been significantly distorted by the strong winds. In the center is a downleg trail that still shows the individual puffs of luminescent material near the top. The bright and expanded glow near the bottom is caused by frictional heating during reentry when TMA frozen to the payload surface is released.

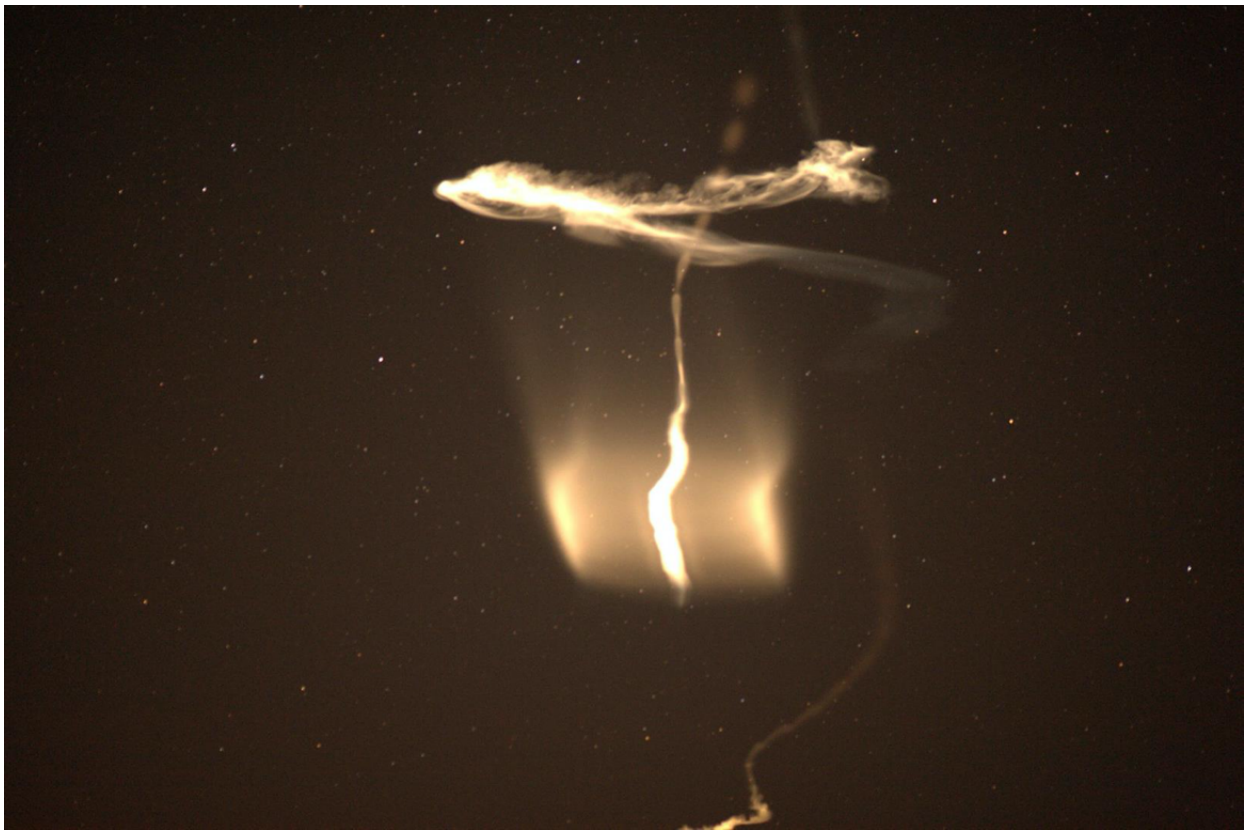

The same trails as seen from Wallops Island looking along the trajectories. Trimethyl aluminum reacts with atomic oxygen to AlO which is chemiluminescent over a broad range of the visible spectrum.

The same trails as seen from Tuckerton, NJ, looking southeastward. The different background star fields provide the reference to determine the exact looking angles.

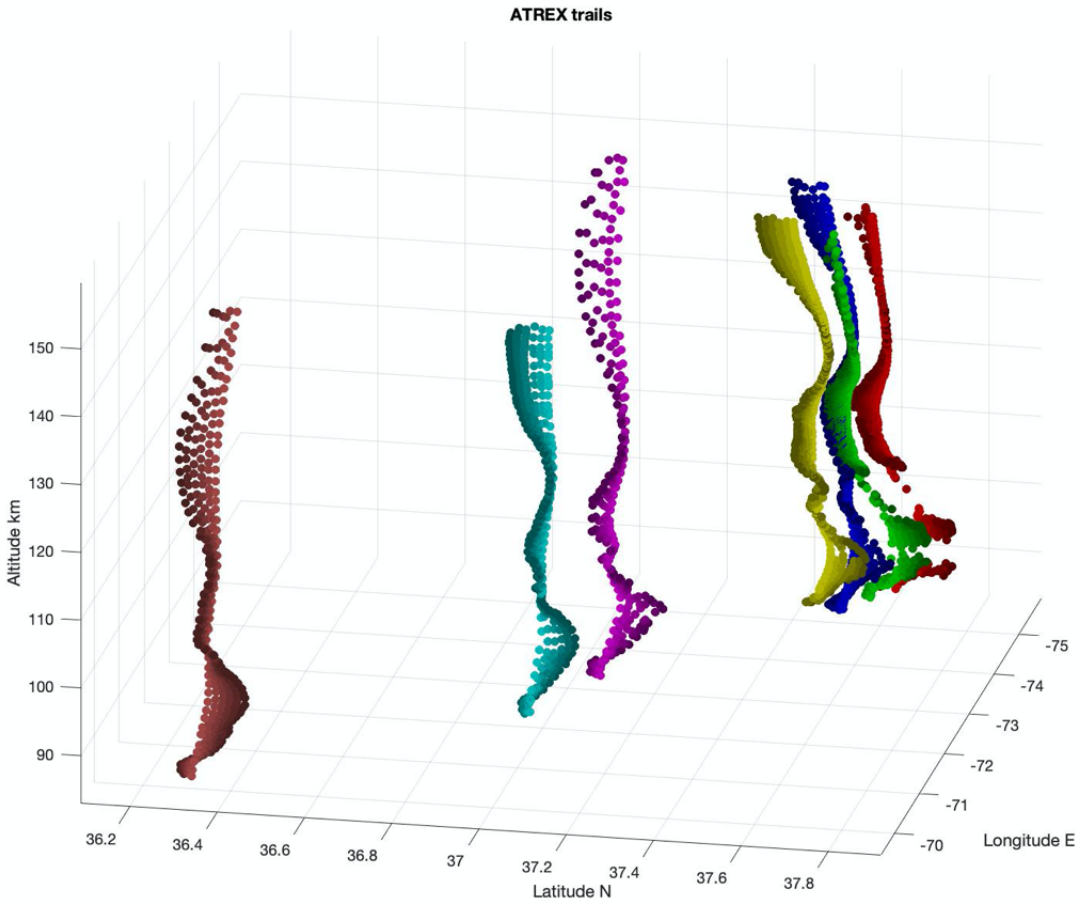

All seven trails were triangulated using pairs of images and the known star fields to determine absolute positions in latitude, longitude and altitude. Each fully developed trail was followed over a period of 90 seconds and 100 to 150 positions were determined per trail.

WIND PROFILES

A linear fit of latitude and longitude over time determines meridional and zonal wind components. Typical position uncertainties are 10-50 meters and typical wind uncertainties are 5 m/s. Where wind speeds are small, however, uncertainties can become much larger. Such data points were removed and replaced by interpolates to achieve a regular altitude grid with 1 km resolution.

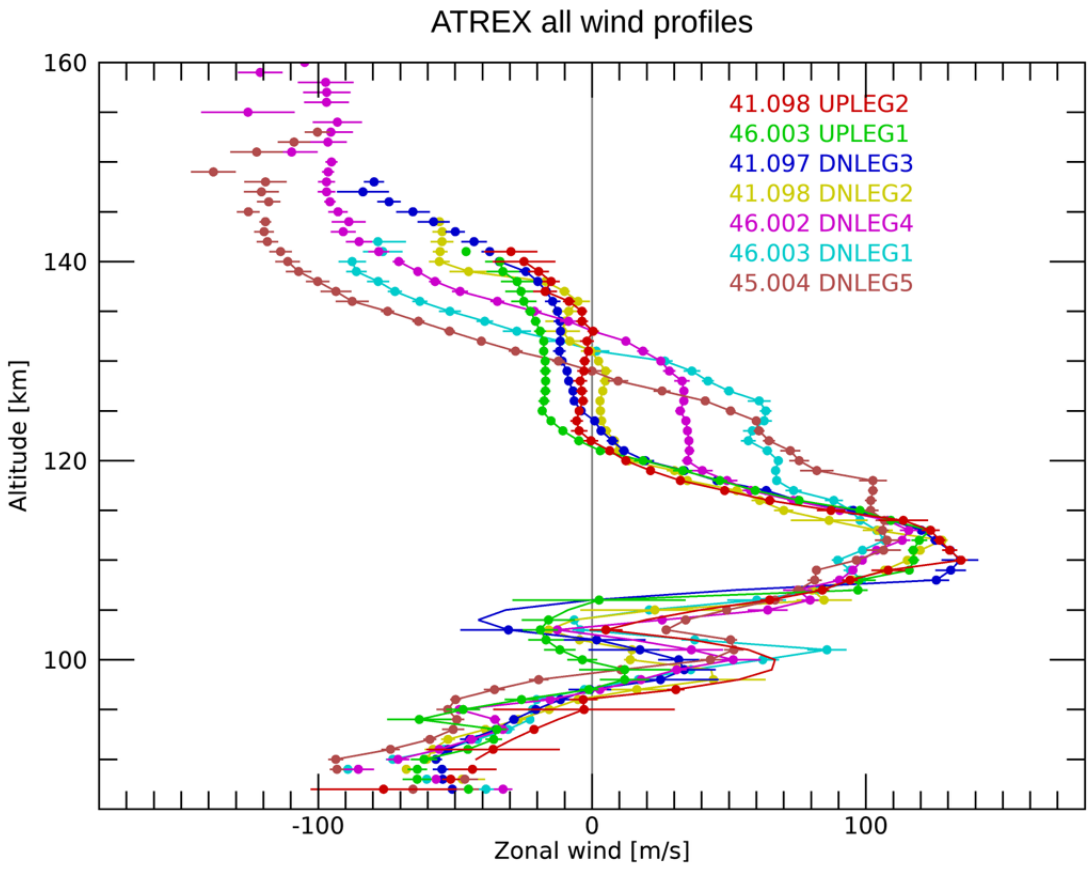

Zonal winds from seven quasi-simultaneous trails. All winds were observed between 09:04 UT and 09:09 UT.

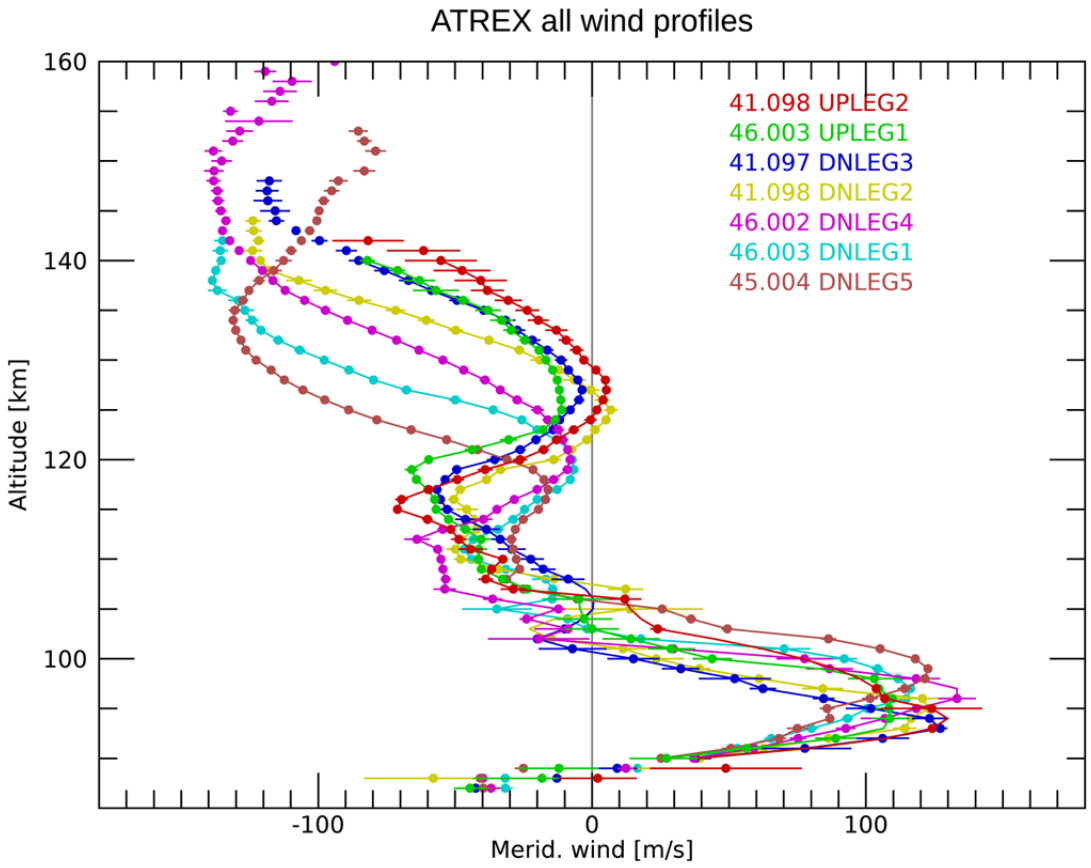

Meridional winds maximize around 95 km. A systematic wavelike variation can be seen above 115 km.

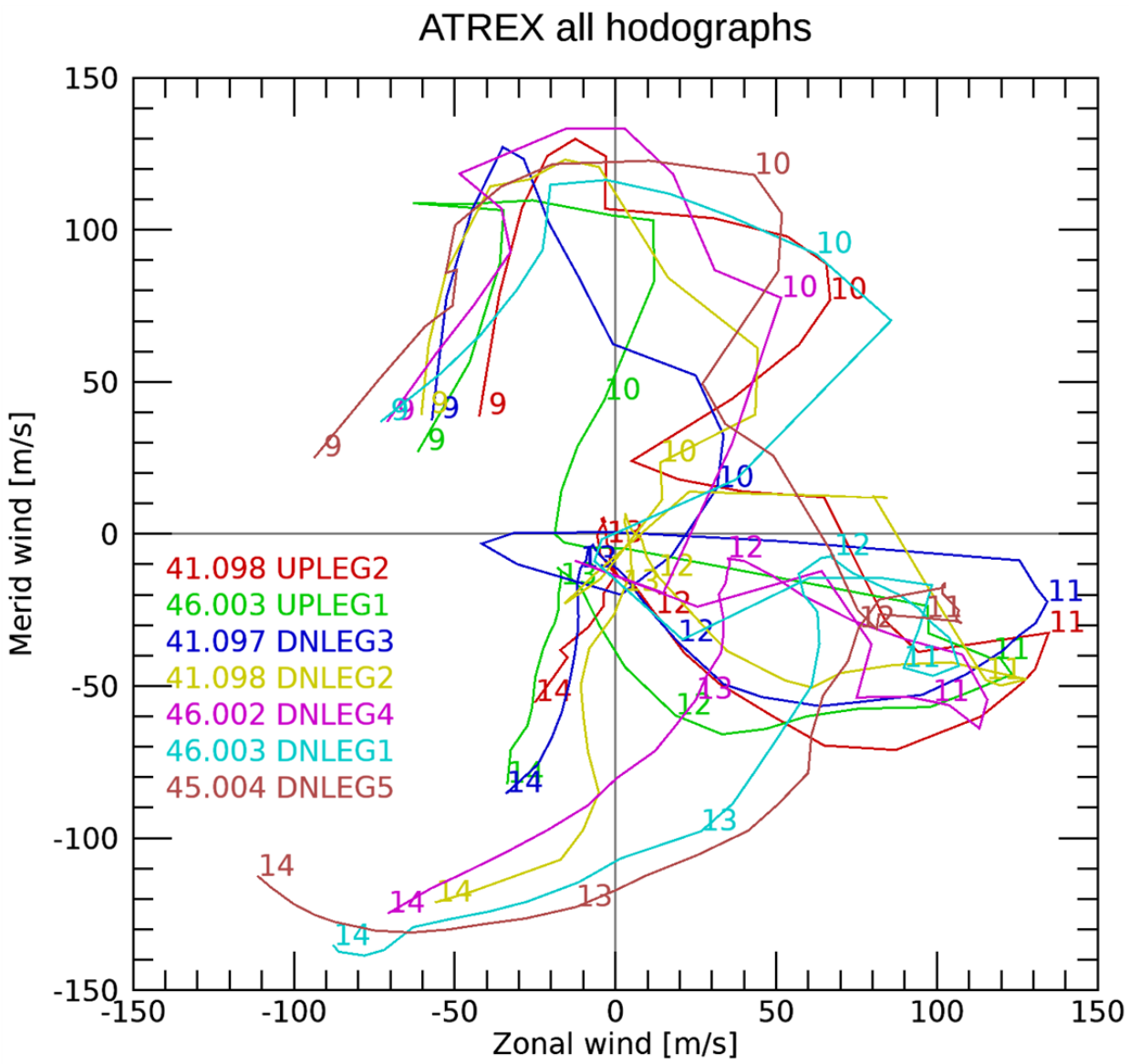

The hodographs indicate that the wind vector rotates clockwise with altitude as is expected for upward propagating gravity waves and tides in the northern hemisphere. Numbers indicate the altitude (in km divided by 10).

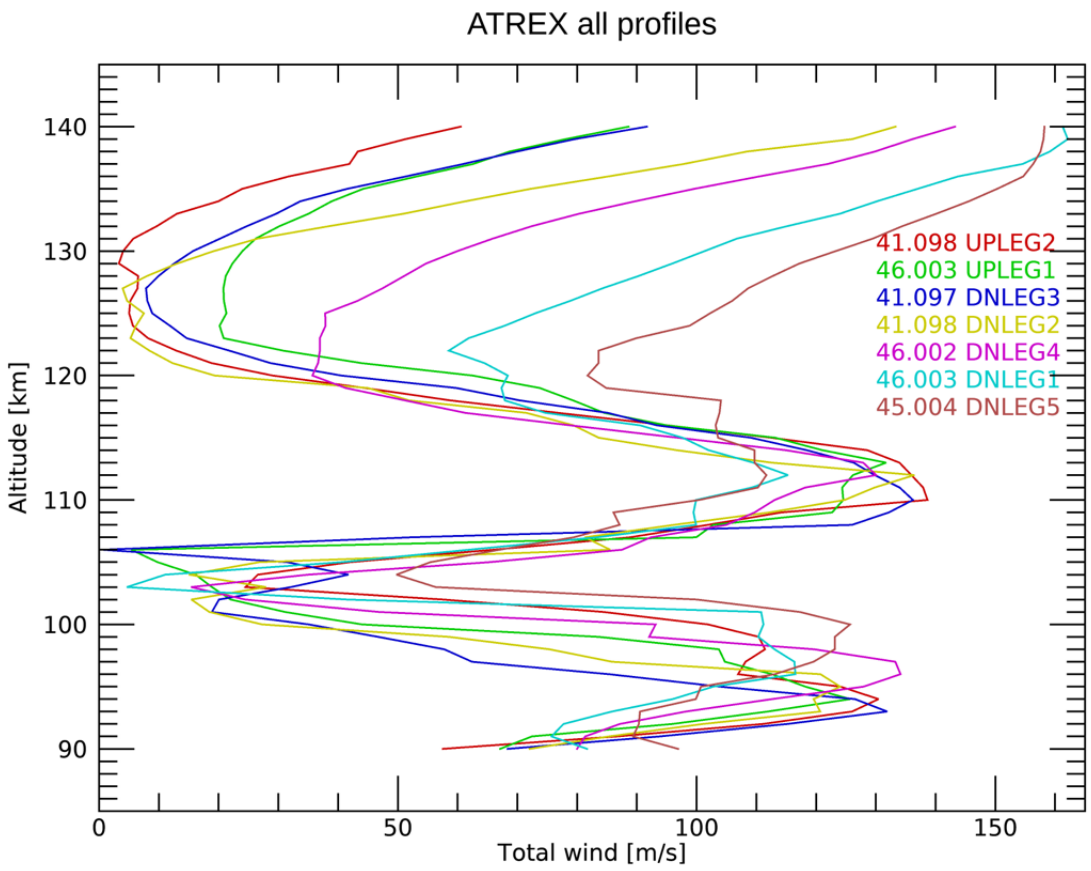

The profiles of **wind magnitude** show two strong maxima with wind speeds well above 100 m/s and a region of relatively weak winds between 100 and 105 km.

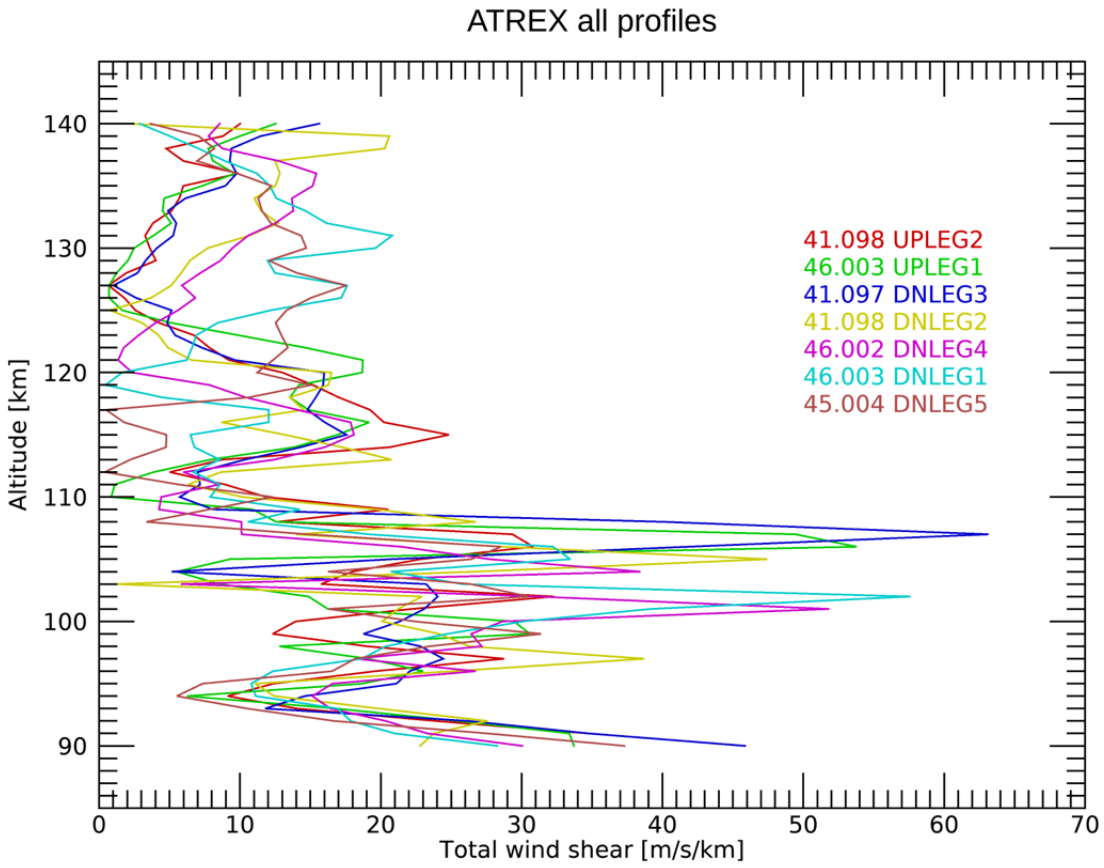

The vertical **wind shear** of the horizontal wind exceeds 40 m/s per km. Given typical buoyancy frequencies, this corresponds to unstable Richardson numbers $Ri = \frac{(2\times10^{-2}\ \mathrm{s}^{-1})^2}{(40\ \mathrm{ms}^{-1}\mathrm{km}^{-1})^2} \sim \frac{1}{4}$

Clear evidence for Kelvin-Helmholtz instabilities has been found in a recent TMA experiment (Mesquita et al., 2020).

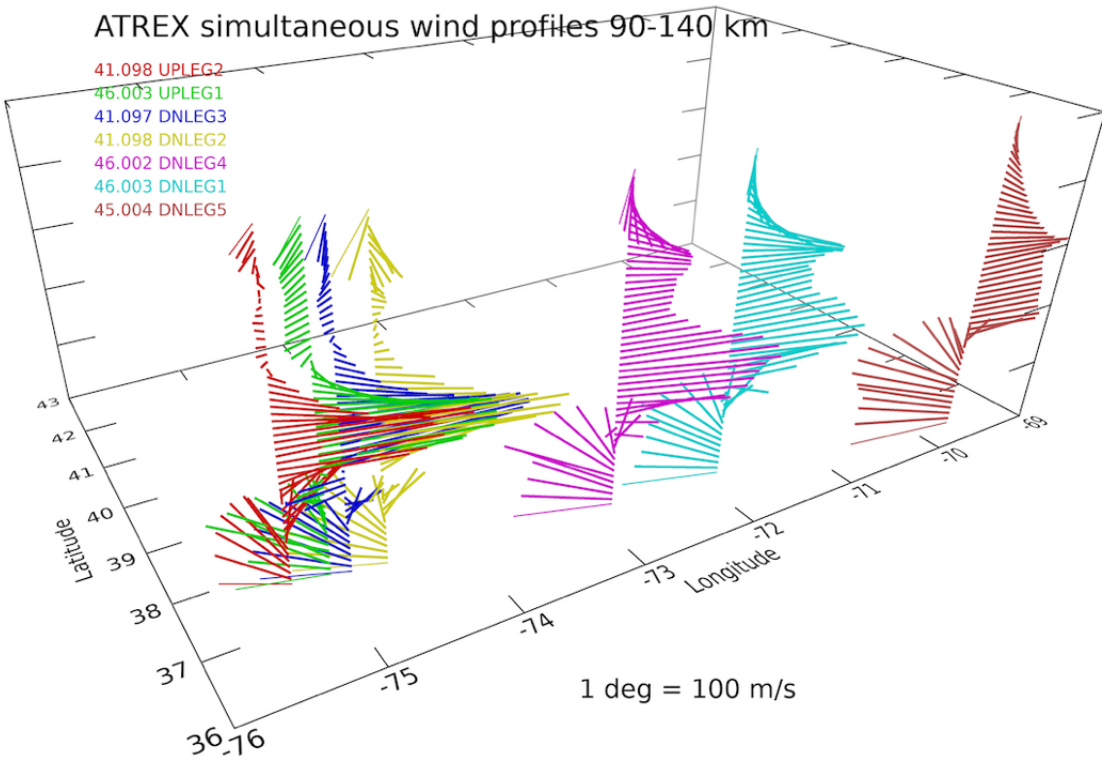

This graph summarizes the wind profiles by plotting wind vectors with their foot point at their respective location in space. Eastward winds are pointing eastward. The rotation of wind vectors and downward phase propagation can clearly be seen.

GRAVITY WAVES AND TIDES

We expect that tidal waves play a dominant role in our lower thermosphere wind profiles observed at lower mid-latitudes. The diurnal migrating tide (mode DE1) maximizes near 95 km, the semidiurnal tide (mode SW2) near 105 km. Furthermore, this experiment was conducted just after spring equinox, when forcing from solar migrating tides is very large.

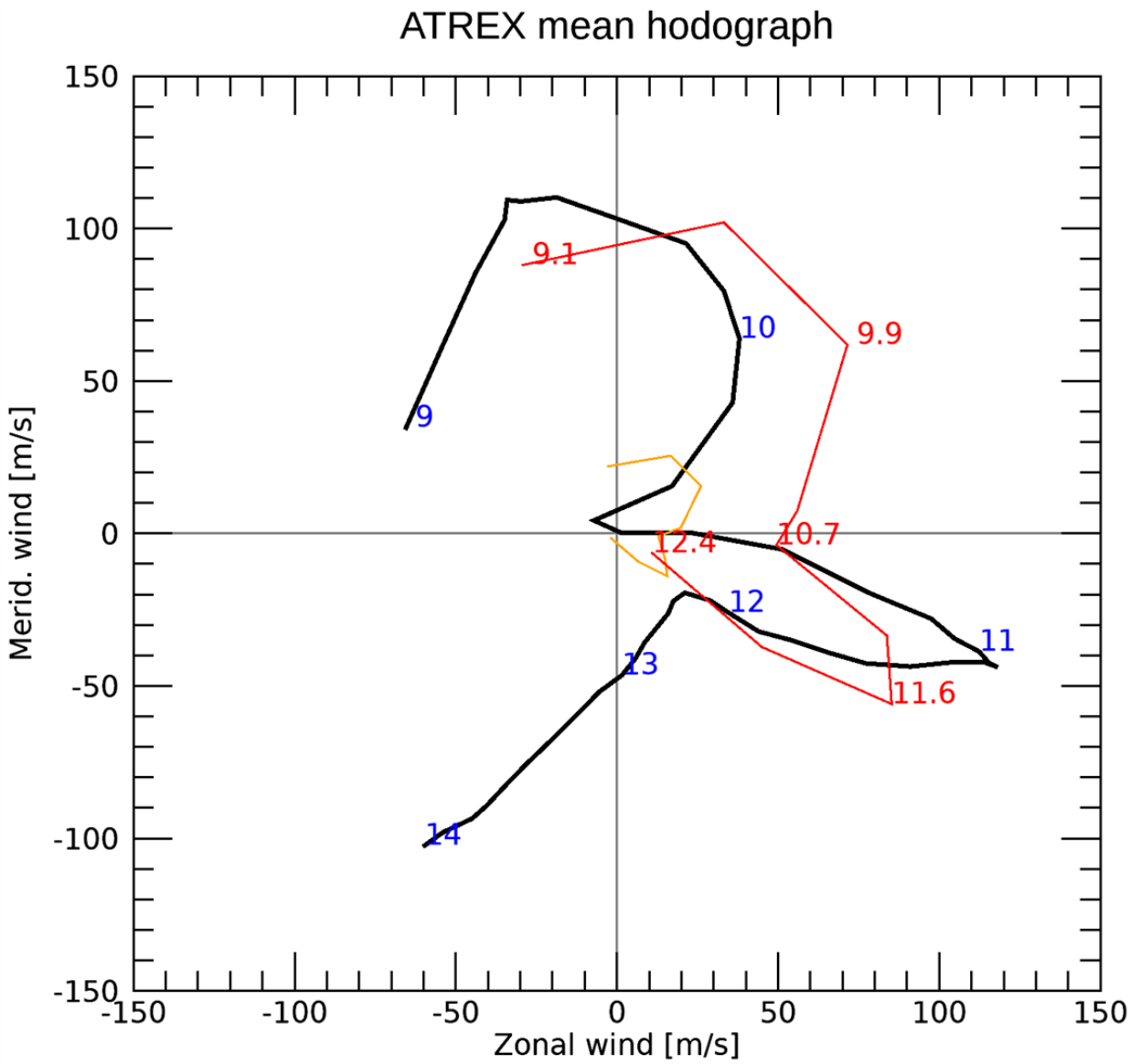

The **mean hodograph** averaging all seven profiles (black) is compared with output from the Global Scale Wave Model (Hagan & Forbes, 2002) for March, 39 N (yellow). GSWM-00 diurnal and semidiurnal amplitudes and a background zonal wind were combined. The model amplitudes are much smaller that what is observed. However, if we scale up all amplitudes by a factor of 3 (red), we find a remarkable similarity to our data between 90 and 124 km! We interpret this that both diurnal and semidiurnal tides were very strong on this day and this location.

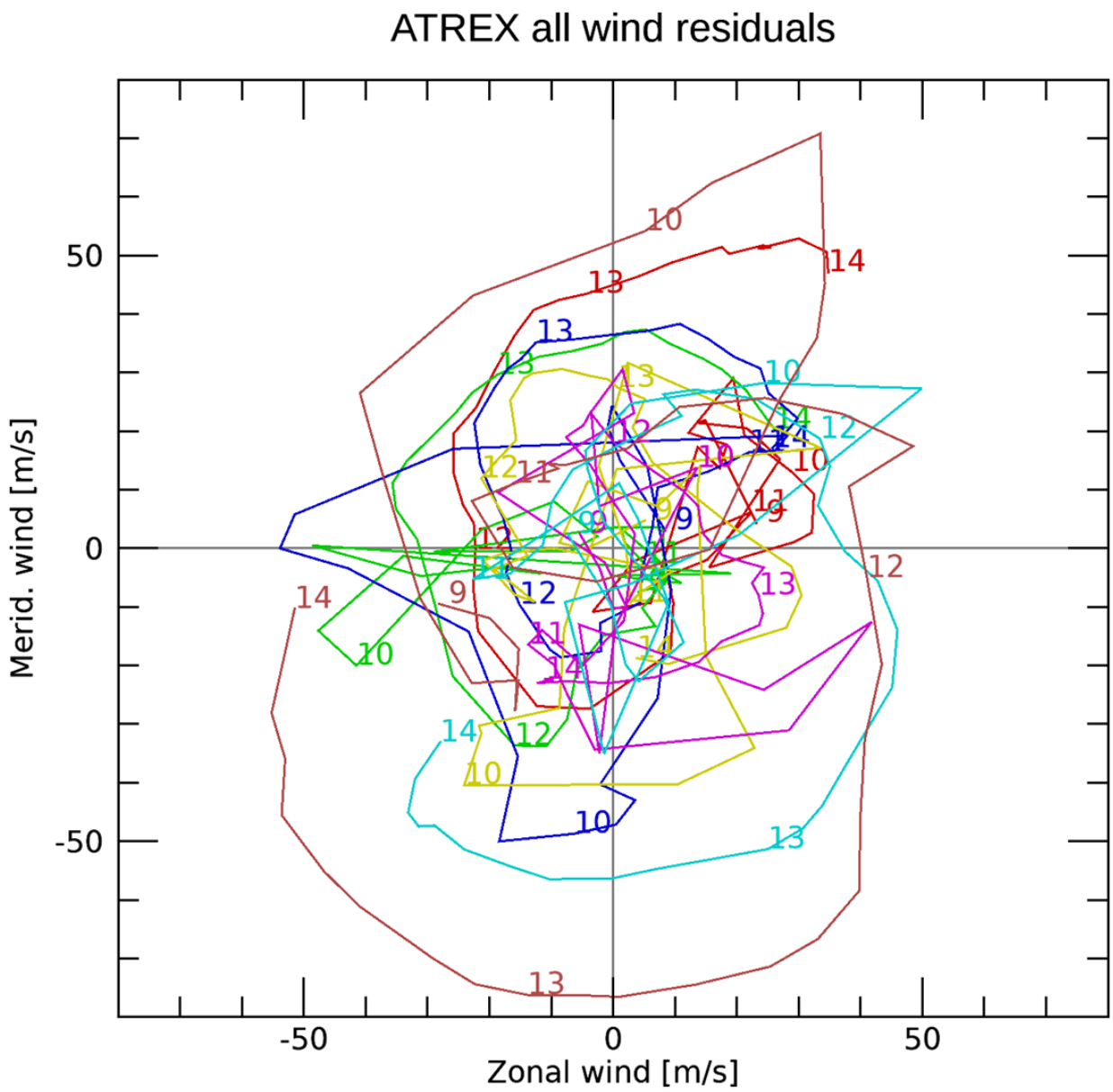

Subtracting the mean from the seven individual profiles leaves these **residuals**.

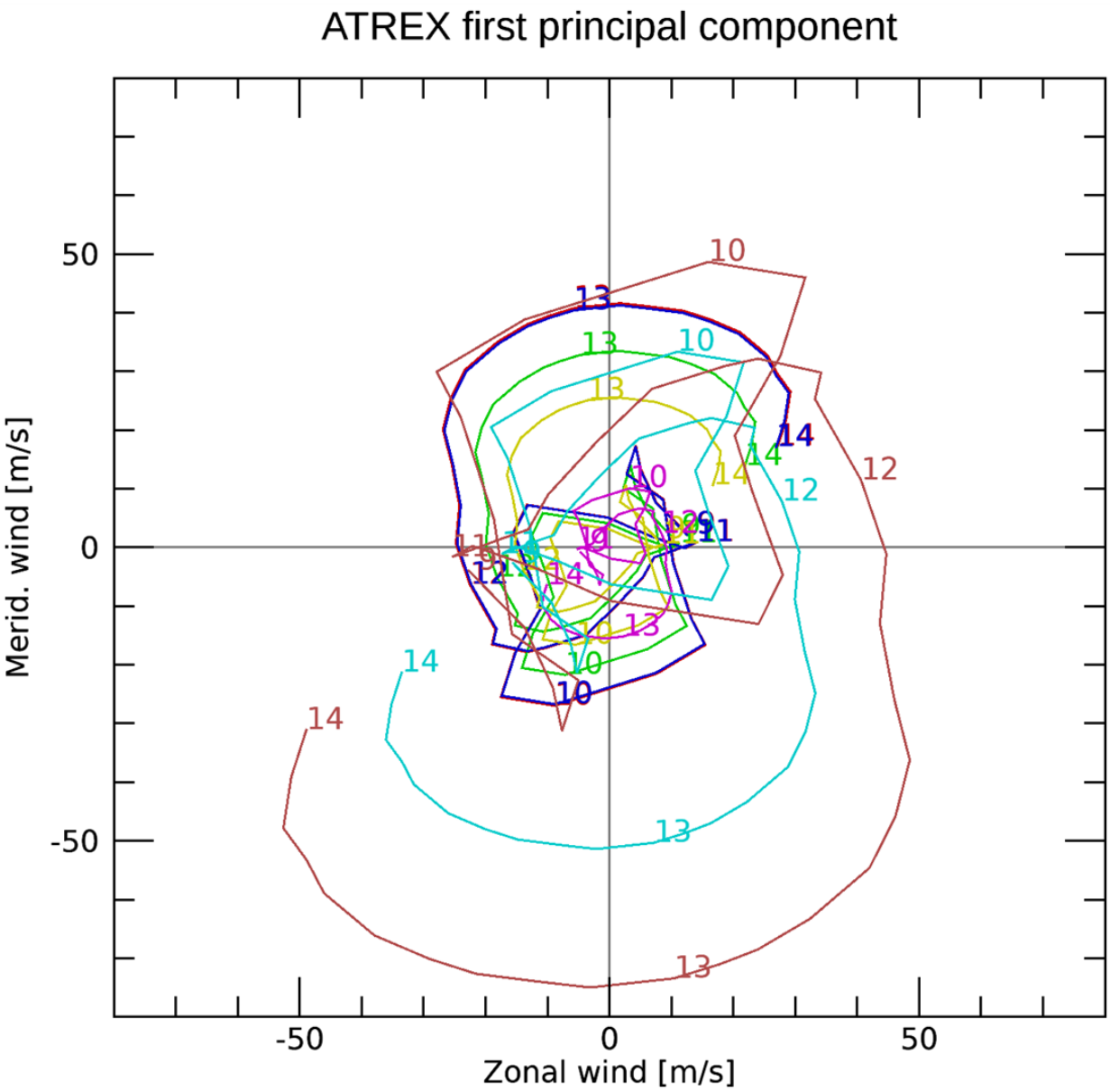

Performing a principal component analysis on the residuals shows a almost circular polarized wave dominating the altitudes above 120 km. 91 % of the variance can be described by the first 3 components. The first principal component is shown above.

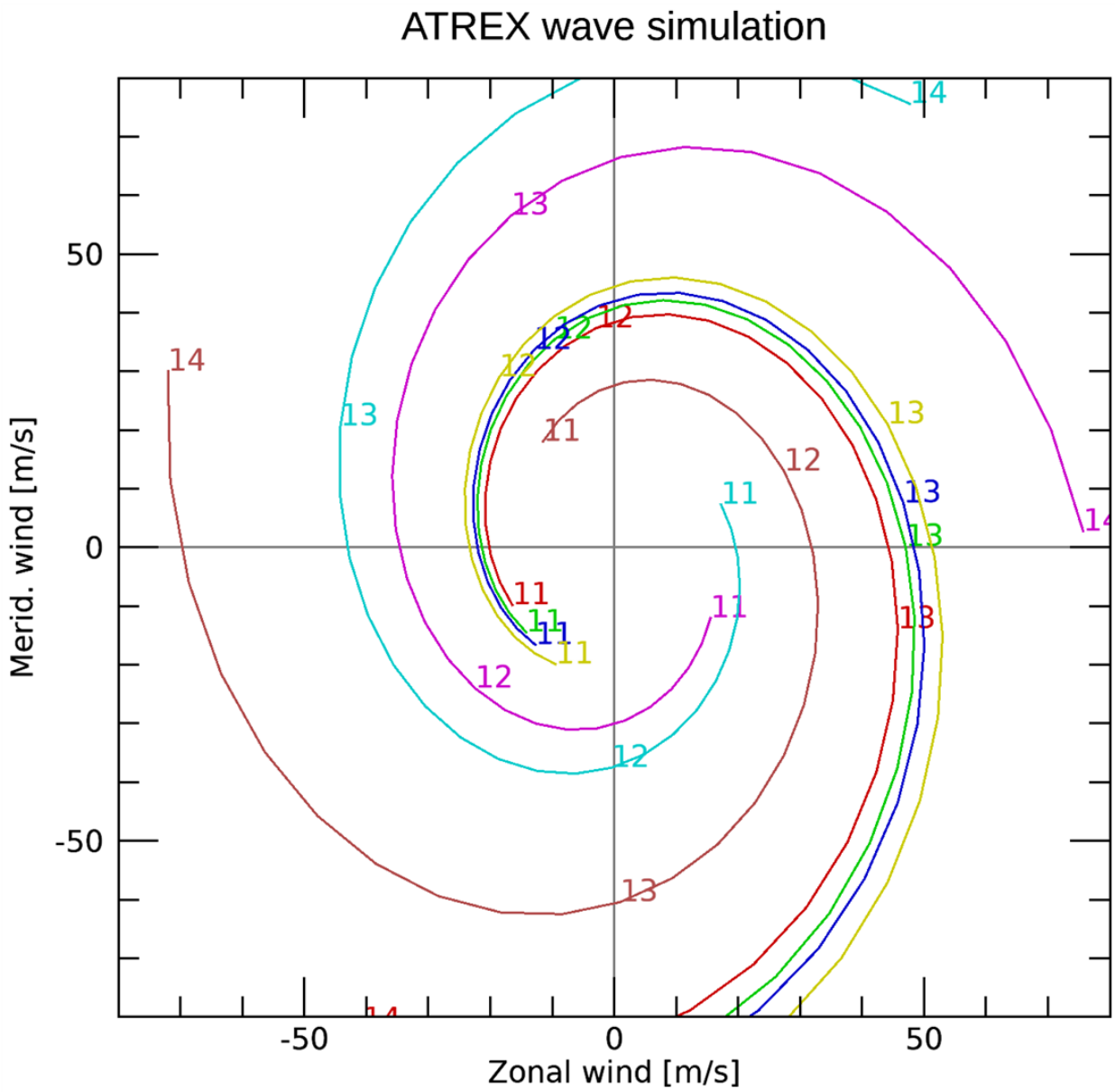

The spatial variation of the wind can be approximated by a monochromatic **inertia gravity wave** with horizontal and vertical wavelengths of ~650 and 33 km, respectively, which is growing using a scale height of 10.5 km. In particular the comparison of the brown spiral with the data shows that the wave is more damped above 130 km. This fit can be further refined by allowing different horizontal wavelengths and taking into account that the observation is not strictly in zonal direction.

The Specified Dynamics runs of the Whole Atmosphere Climate Community Model (here **SD-WACCM-X 2.1**, Liu et al., 2018) can produce realistic tidal amplitudes, although matching for a particular location is not expected. Hourly outputs of U and V were fitted with sine and cosine waves of 24 and 12 hour periods. In the figure these are combined into a total horizontal wind amplitude and shown for the day of the experiment, 27 March 2012.

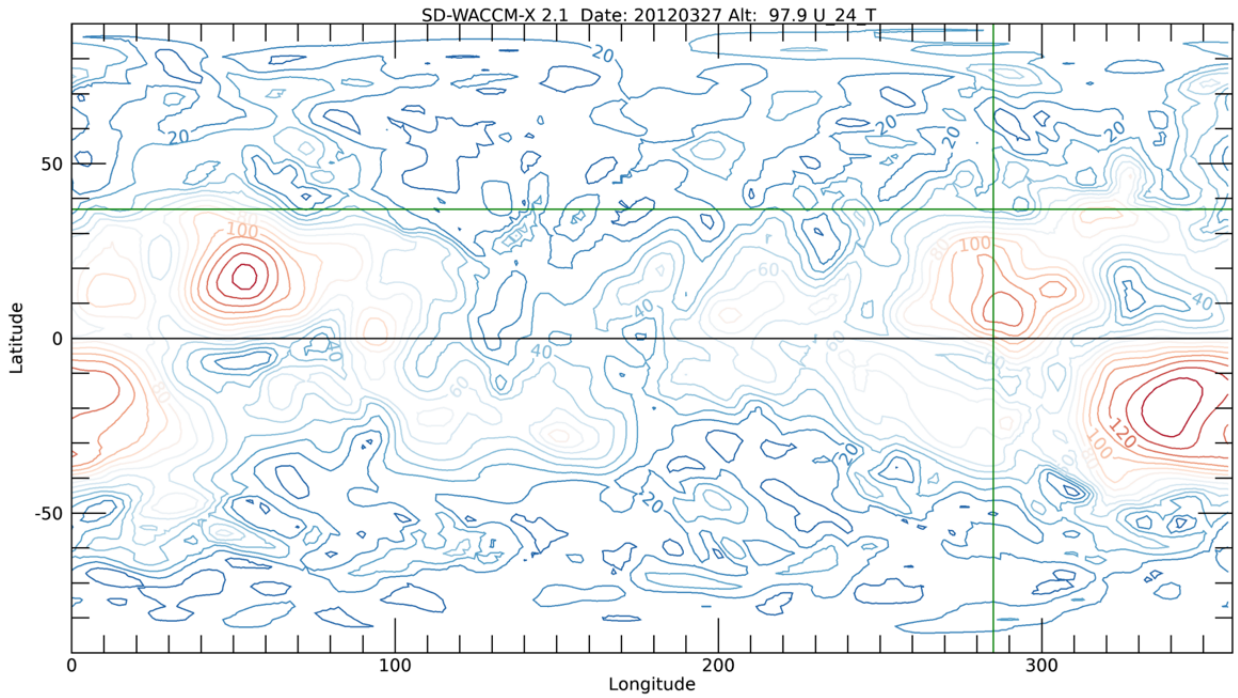

The diurnal (24 hour) amplitude is mostly confined between 40 N and 40 S and is dominated by the DE1 mode. Hots spots of 100 m/s and more are produced near 20 degrees latitude and around several longitudes. The intersection of the green lines mark the location of our wind measurements.

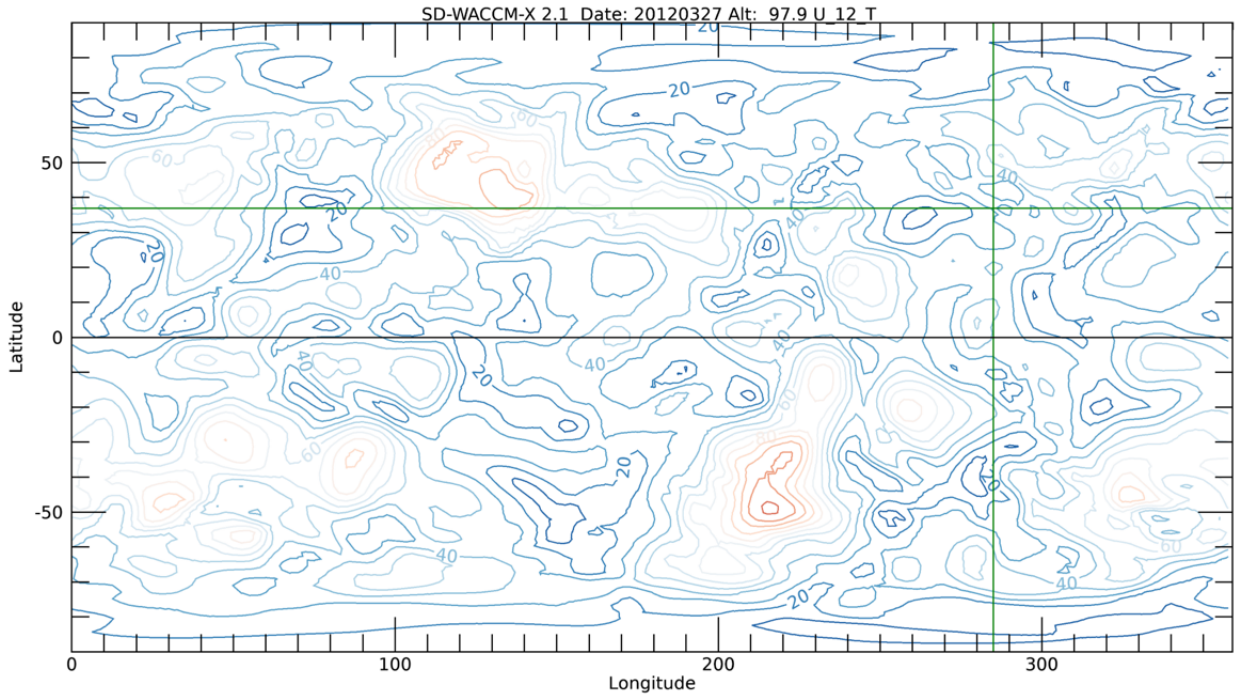

The semidiurnal (12 hour) magnitudes extend to midlatitudes and maximize near 50 degrees latitude. Again, magnitudes can exceed 100 m/s in certain locations. Our observations of tidal wind amplitudes of 100 m/s and more support such model simulations.

MESOSCALE VARIABILITY

In order to explore mesoscale variabilitity, we estimate the second-order structure function of our data set for different altitude intervals. We follow the methodology of Cho and Lindborg (2001) who calculated second- and third-order structure functions in the upper troposphere and lower stratosphere based on a large data set of 8000 commercial aircraft flights.

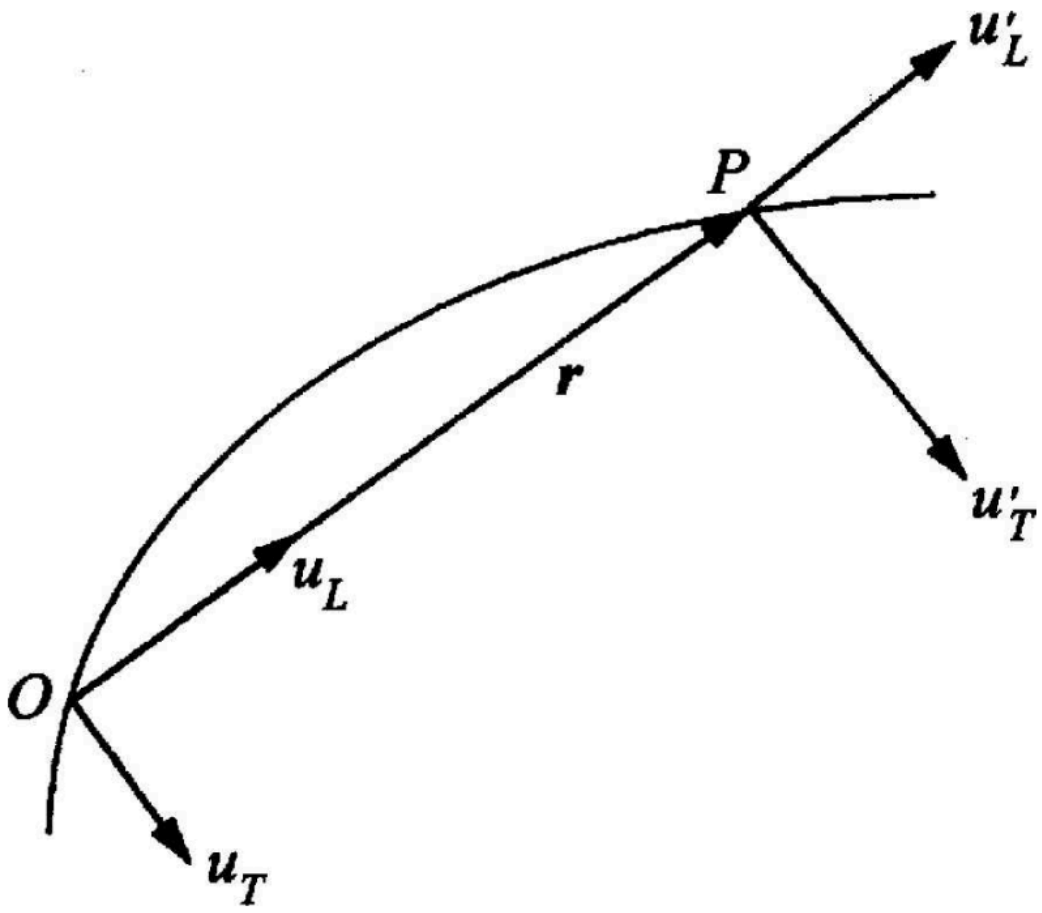

Each pair of vector wind measurements ***u, u'*** is projected along and perpendicular to the separation vector ***r***, (see figure above) and the longitudinal and transverse differences are squared (and averaged) to yield $\langle \delta u_L \cdot \delta u_L \rangle$ and

$\langle \delta u_T \cdot \delta u_T \rangle$ which is graphed vs. separation (spatial lag).

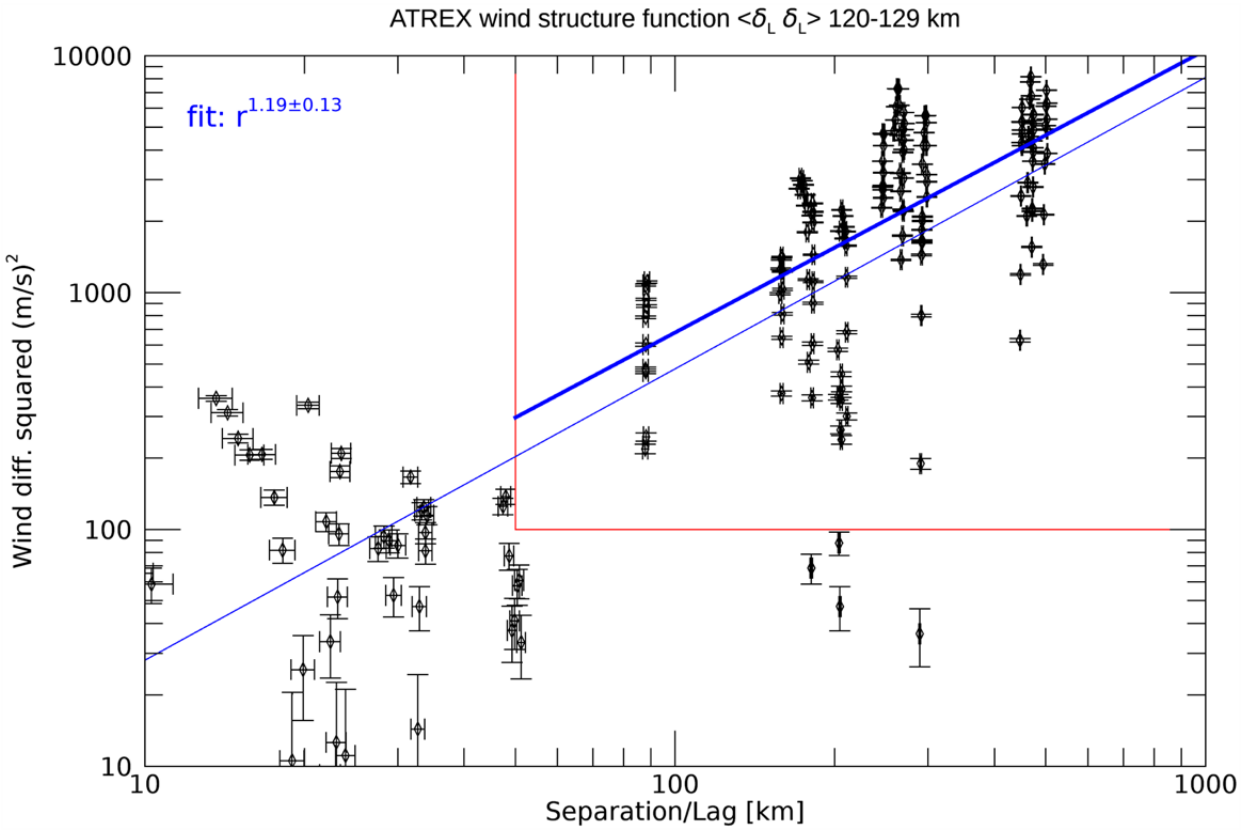

From seven flights, 21 values were constructed for each altitude. The example above shows 210 data points for 120 to 129 km altitude. We did not bin and average the data, and show the full scatter of values. Position and wind uncertainties of max. 1 km and 5 m/s are indicated by the error bars. The thick blue line is a power law fit to scales above 50 km and excluding smaller wind differences. The thin blue line is a fit to all data. The squared differences increase clearly with lag and has a power law exponent of 1.19±0.13.

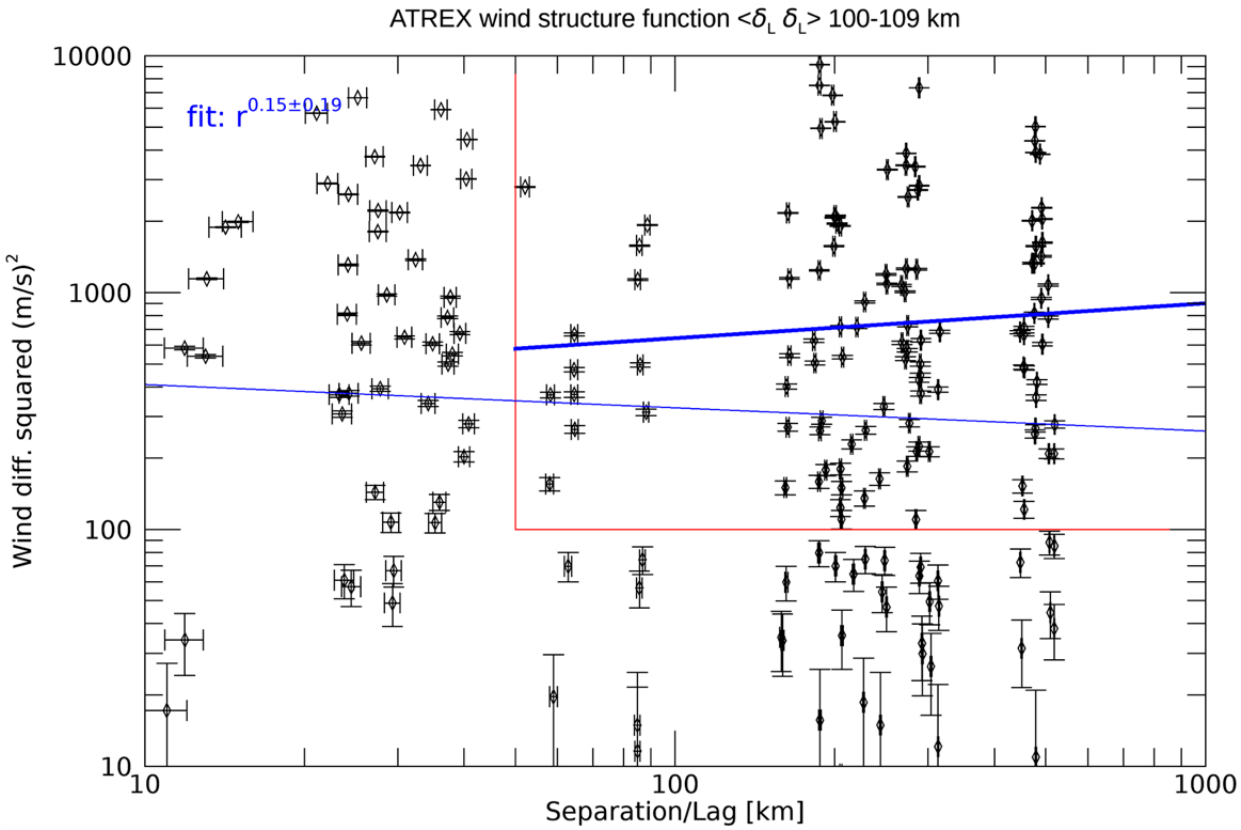

A second example shows the same analysis for the interval 100-109 km Within the uncertainty, the power exponent is independent of lag (exponent 0.15±0.19), which would also be expected if the wind data were a random sample of white noise.

Longitudinal and transverse structure functions showed consistent exponents. The power law coefficients for the second-order structure functions for all intervals were:

Altitude (km)	longitudinal	transverse
90-99	0.79±0.17	0.52±0.16
100-109	0.15±0.19	0.28±0.20
110-119	0.57±0.14	0.73±0.16
120-129	1.19±0.13	1.38±0.21
130-139	0.79±0.16	1.44±0.16

The second- and third-order structure functions for isotropic 3-D turbulence have been shown to follow power laws (Kolmogorov, 1941)

$$\langle(\delta u_L)^2\rangle = C_2\epsilon^{2/3}r^{2/3} \text{ and } \langle(\delta u_L)^3\rangle = -\frac{4}{5}\epsilon r$$

The transverse structure functions follow the same power laws, but with different coefficients. They assume a single energy input ε at larger scales and a forward (downscale) cascade of energy to the smallest dissipative scales. The $r^{2/3}$ law is equivalent to the well-known $k^{-5/3}$ dependence of the 1-dimensional energy spectrum.

For two-dimensional turbulence, energy and vorticity are conserved (Kraichnan, 1967). From the scale, where energy is injected, two inertial cascades originate: a forward cascade of enstrophy (which is half the vorticity squared) and energy spectrum k^{-3} and an upscale (reverse) cascade of energy (also with energy spectrum $k^{-5/3}$). It is the -5/3 spectrum in the atmosphere at mesoscales that

has been controversially discussed for decades: Is it two-dimensional turbulence leading to the formation of “pancake” vortices at mesoscales? Or is it a quasi-three-dimensional process of interacting gravity waves that cascades energy downward? Or both?

Lindborg (1999) derived formulas for the structure functions based on different scenarios of forcing. He specifically considered energy input at large scales (~1000 km) and small scales (~ 1 km), so that both inertial ranges overlap. The second-order longitudinal structure functions can be written

$$\langle (\delta u_L)^2 \rangle = a_1 r^{2/3} + b_1 r^2 - c_1 r^2 \ln r$$

This formula (and one for the third-order structure function) were fitted to a large database of aircraft measured winds for separations from 2 to 2000 km (Cho and Lindborg, 2001). The transition from $r^{2/3}$ to r^2 was observed at ~100 km. From the third-order structure functions, which were negative between 10 and 100 km, it was concluded that the energy cascade was downscale at mesoscales. In later publications, the theory was also applied to high-resolution atmospheric models (e.g., Augier and Lindborg, 2013).

How can this be applied to the lower thermosphere? Our results show that each 10 km deep region (which is more than the range of all aircraft altitudes) exhibits a variety of lag dependence. Five exponents are compatible with $r^{2/3}$(or $k^{-5/3}$). The presence of a singular large scale gravity wave affected the exponents above 120 km. The region with the strongest wind shears (100-110 km) showed the smallest dependence on lag. On the other hand, (see previous panel), the average wind structure up to 120 km, including the strong wind shears, was compatible with large-scale tides, as the comparison with the tidal model suggests. An alternative type of analysis using structure in the trail brightness as scalar tracer showed an transition scale near 100 km from quasi 3D to 2D behavior (Roberts & Larsen, 2014). Our analysis is able to measure wind structure directly and its variability in different altitudes, but techniques that produce much larger datasets of thermospheric winds are needed to study universal power laws at mesoscales.

DISCLOSURES

This work was partially supported by NASA under Grant NNX11AE17G. SD-WACCM-X data were provided by Nick Pedatella at NCAR and downloaded from https://www.earthsystemgrid.org/. GSWM-00 data were downloaded from http://www.hao.ucar.edu/modeling/gswm/gswm.html.

ABSTRACT

The Anomalous Transport Experiment (ATREX) comprised seven quasi-simultaneous observations of lower thermospheric winds, horizontally separated by up to 600 km, on 27 March 2012, 0900 UT. Zonal and meridional wind profiles were obtained with five sounding rockets launched from Wallops Island (38 N, 75.5 W) releasing seven trimethyl aluminum trails which were observed from three cameral sites.

The wind profiles exhibit deep coherent wave structures between 85 and 140 km, dominated by very strong diurnal and semidiurnal tides below 120 km. The total wind amplitude exceeds 100 m/s, three times the value from the Global Scale Wave Model. In addition, a large scale, vertically propagating and growing, inertia-gravity wave, most visible above 120 km, has been isolated by empirical orthogonal function analysis.

The region between 100 and 110 km shows the largest mesoscale variability of winds and wind shears, often exceeding 40 m/s/km. We will present an estimation of the structure function for wind fluctuations and possible evidence for stratified mesoscale turbulence.

REFERENCES

Augier, P., & Lindborg, E. (2013). A new formulation of the spectral energy budget of the atmosphere, with application to two high-resolution general circulation models. Journal of the atmospheric sciences, 70(7), 2293-2308.

Cho, J. Y., & Lindborg, E. (2001). Horizontal velocity structure functions in the upper troposphere and lower stratosphere: 1. Observations. Journal of Geophysical Research: Atmospheres, 106(D10), 10223-10232.

Hagan, M. E., & Forbes, J. M. (2002). Migrating and nonmigrating diurnal tides in the middle and upper atmosphere excited by tropospheric latent heat release. Journal of Geophysical Research: Atmospheres, 107(D24), ACL-6.

Kolmogorov, A. N. (1941; transl. 1991). Dissipation of energy in the locally isotropic turbulence. Proceedings of the Royal Society of London. Series A: Mathematical and Physical Sciences, 434(1890), 15-17.

Kraichnan, R. H. (1967). Inertial ranges in two−dimensional turbulence. The Physics of Fluids, 10(7), 1417-1423.

Larsen, M. F. (2002). Winds and shears in the mesosphere and lower thermosphere: Results from four decades of chemical release wind measurements. Journal of Geophysical Research: Space Physics, 107(A8), SIA-28.

Lindborg, E. (1999). Can the atmospheric kinetic energy spectrum be explained by two-dimensional turbulence?. Journal of Fluid Mechanics, 388, 259-288.

Liu, H. L., Bardeen, C. G., Foster, B. T., Lauritzen, P., Liu, J., Lu, G., ... & Qian, L. (2018). Development and validation of the Whole Atmosphere Community Climate Model with thermosphere and ionosphere extension (WACCM−X 2.0). Journal of Advances in Modeling Earth Systems, 10(2), 381-402.

Mesquita, R. L., Larsen, M. F., Azeem, I., Stevens, M. H., Williams, B. P., Collins, R. L., & Li, J. (2020). In Situ Observations of Neutral Shear Instability in the Statically Stable High−Latitude Mesosphere and Lower Thermosphere During Quiet Geomagnetic Conditions. Journal of Geophysical Research: Space Physics, 125(8), e2020JA027972.

Roberts, B. C., & Larsen, M. F. (2014). Structure function analysis of chemical tracer trails in the mesosphere−lower thermosphere region. Journal of Geophysical Research: Atmospheres, 119(11), 6368-6375.